Phys. Status Solidi C **14,** No. 7, 1700114 (2017) / **DOI** 10.1002/pssc.201700114

physica status solidi c
www.pss-c.com
current topics in solid state physics

Luminescent and electrical properties of oxygen-implanted silicon

Denis Danilov[*,1], Oleg Vyvenko[,1], Anton Loshachenko[1], Boris Ber[2], Dmitrii Kasantsev[2], and Nikolay Sobolev[***,2]**

[1] St. Petersburg State University, Universitetskaya nab. 7/9, 199034 St. Petersburg, Russia
[2] Ioffe Institute, Polytekhnicheskaya 26, 194021 St. Petersburg, Russia

Received 1 March 2017, accepted 24 May 2017
Published online 13 June 2017

Keywords luminescence, oxygen ion implantation, silicon

[*] Corresponding author: e-mail d.danilov@spbu.ru, Phone: (+7) 812 428 4733, Fax: (+7) 812 428 7240
[**] e-mail vyvenko@nano.spbu.ru
[***] e-mail nick@sobolev.ioffe.rssi.ru

Light emitting diodes with an active defect-rich region produced by oxygen implantation and a subsequent multistep annealing of silicon wafers were investigated by means of transmission electron microscopy, SIMS, capacitance voltage, deep level transient spectroscopy, electroluminescence (EL), and cathodoluminescence (CL) techniques. The properties of two groups of n-based samples with and without thermal pre-treatment at 1000 °C for 15 min were compared regarding their defect structure, defects electrical activity, luminescent spectra as well as the impact of prolonged intense electron irradiation. The observed difference in the properties of such groups was explained by a difference in the density and oxygen content of oxygen-related defects. A significant distinction between EL and CL spectra at low excitation levels was found and interpreted to be due to particular defect kinds in near-surface and the deepest layers of the implanted region. The blue shift of EL spectra upon excitation increase reported previously is explained by the increase of penetration depth of the holes and specific depth distribution of the defects of different kinds.

1 Introduction Defect-related luminescence (DRL) in silicon in the spectral region 0.8 eV attracts attention of investigators as a possible candidate for CMOS compatible light source [1–5]. It is well known that the main sources of radiative transitions in this energy range are dislocations and/or oxygen precipitates [6]. One of the industrially compatible technological approaches to produce DRL-based light emitting devices (LED) is ion implantation with subsequent high-temperature treatment [7–9].

Recently we reported results of characterization of defect structure, electrical properties, and DRL of LEDs with the active defect-rich region produced by oxygen implantation and a subsequent multistep annealing of silicon wafers [10]. It was found that defect-rich regions possess an embedded positive charge in both n- and p-type of the samples whose origin was ascribed to oxygen precipitates (OPs). The presence of that charge in the implanted region of p-based LED gave rise to the apparent conductivity type conversion and to a significant increase of free electron concentration in n-based LEDs. A significant difference in the shape and in the excitation dependence of luminescence spectra as well as in the properties of DLTS signals was found between p- and n-type samples. From an analysis of the obtained data the DRL band centered at 0.79 eV, 0.805 eV and the broad band above 0.81 eV was ascribed to small oxygen precipitates in the vicinity of dislocations, dislocation-related states, and to large OPs, respectively. However, the observed evolution of electroluminescence (EL) spectra with its drastic blue shift upon excitation was not understood unambiguously.

In this work, we extended our previous research [10] applying additionally secondary ion mass spectrometry (SIMS) for oxygen concentration depth profiling as well as cathodoluminescence (CL) in scanning electron microscope (SEM) for characterization of DRL. Besides we investigated the impact of an intense and prolonged electron irradiation in SEM on the properties of our OP-rich samples bearing in mind that such kind of the treatments is known to be able to

change significantly electronic properties of massive silicon dioxide [11].

We found significant differences between the profiles of the total oxygen concentration and defect-related electrical activity, between spectral DRL response of the near surface and bottom-implanted regions as well as between the sensitivities of small and large OPs to the electron irradiation.

2 Experimental

2.1 Samples The samples were prepared from the phosphorus-doped Cz-Si wafer with the doping and oxygen concentration of about $10^{15}\,cm^{-3}$ and $1.1\times10^{18}\,cm^{-3}$, respectively. The wafer was subjected to the successive oxygen implantation with the ion energies 350/225/150 keV and with doses $1.5\times10^{15}/0.9\times10^{15}/0.7\times10^{15}\,cm^{-2}$, respectively to create nearly constant oxygen concentration in the region from 300 to 800 nm from the surface. After the implantation, the samples were exposed to a multistep annealing described in details in Ref. [12]. Two groups of the samples were prepared which were distinguished by presence or absence of first treatment at 1000 °C for 15 min that will be denoted as nO_4 or nO_3, respectively. This step released oxygen captured with initial traps. The rest three treatments consisting of the annealing at 650 °C for 7 h, at 800 °C for 4 h, at 1000 °C for 6 h for the grow of precipitates were identical for both groups of the samples. The first three annealing were carried out in the Ar ambiance, the last fourth annealing was carried out in chlorine-contained atmosphere (CCA) [13].

Ohmic contacts and p^+n junctions were created by vapor–phase epitaxy of polycrystalline silicon highly doped with P and B onto the back sides and the faces of the samples, respectively. After the first set of measurements, the samples were kept in SEM under scanning electron beam with energy of 30 kV and the beam current of 20 nA for 12 h at the temperature 70 K.

2.2 Results TEM, SIMS Figure 1 represents the comparison of dark-field cross-sectional transmission electron microscopy (TEM) image of the defect structure with SIMS oxygen concentration profiles as well as with the profile calculated with SRIM routine. The horizontal scale in Fig. 1 started from the sample surface. TEM image in Fig. 1 was obtained on the sample with the first 1000 °C pre-annealing step and was similar to the sample without such step in its main features. Careful examination of the TEM image reveals that the implanted region can be divided into three layers with qualitatively different defect structure marked in Fig. 1 as TD, SD + OP, and OP. TD contains threading dislocations crossing the sample surface, SD + OP is the region with diverse structural defects of high density and with oxygen precipitates, OP is the region containing predominantly individual oxygen precipitates.

SIMS spatial distribution of oxygen concentration in the samples without 1000 °C pre-annealing (stars in Fig. 1) was similar on one calculated with SRIM routine (white solid line in Fig. 1). This indicates that the most of the implanted oxygen remained within initially implanted region despite the performed three-step thermal treatment. The rapid increase of oxygen concentration at the surface appears to be an artefact due to the presence of surface oxide.

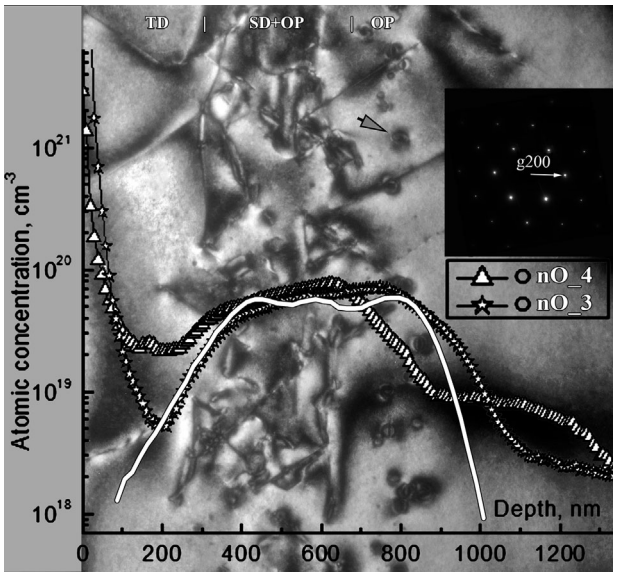

Figure 1 Oxygen concentration profiles obtained by SIMS on nO_3 (stars) and on nO_4 (triangles), calculated by SRIM (white solid line). Background: dark-field cross-sectional TEM image of the sample nO_4 with 1000 °C pre-annealing. Black arrow marks a big OP. TD – threading dislocations region, SD + OP – the region of structure defects and oxygen precipitates, OP – the region of free oxygen precipitates.

The impact of the 1000 °C pre-annealing is clearly seen from the comparison of SIMS measurement profiles for nO_4 and nO_3 samples. Oxygen concentration increased at the surface in TD layer, remained the same as in the sample nO_3 within SD + OP layer and reduced in the deeper part forming a shoulder propagating from the edge of OP layer deeper than 1200 nm. The latter behavior might be interpreted partly due to oxygen out-diffusion into the bulk from interstitial rich area caused by a high oxygen diffusion coefficient at 1000 °C ($\sim10^{-12}\,cm^2\,s^{-1}$) but could be partly also an artefact that will be discussed below.

The dislocation density in TD area estimated from multiple TEM images was as high as $10^{11}\,cm^{-2}$ in both groups of the samples. According to SIMS data, the oxygen concentration in this area was not less than $10^{19}\,cm^{-3}$ but no indication of the presence of oxygen precipitates was found. This implies that significant part of oxygen in this area forms complexes invisible for TEM.

The depth of the uniform layer of big OPs of 700–900 nm corresponds to the projection range (Rp) of oxygen ions with energy of 350 keV as it is seen as the deepest bump on the SRIM simulation profile in Fig. 1. In the sample subjected to the first homogenized annealing at 1000 °C, the density of the big OPs in that area was significantly higher in spite of the lower value of retrieved

from SIMS data. On the other side, coincidence of the SRIM and SIMS concentration in this layer indicates that in the sample without first step the most of the oxygen possess the form invisible for TEM.

Besides, rather rare OPs were found in the area from 1000 to 1200 nm in both kinds of the samples despite significant difference of SIMS data. The reason for such discrepancy might be that SIMS provides lower density and elongated profile due to reduced oxygen evaporation rate from large OPs similar to the artefact due to the presence of surface oxide. Trying to find a confirmation of this idea, we estimated roughly the amount of oxygen in the OPs layer 700–900 nm from the average size and density of OPs in the sample nO_4. It was few of $10^{14}\,cm^{-2}$, that correlated by the order of magnitude with the amount of oxygen with SIMS data in the entire region 800–1200 nm.

A high density of extended defects such as dislocations, dislocation dipoles, Frank loops with embedded stacking faults can be seen in the region SD + OP situated at the depths from 300 to 700 nm. The SIMS oxygen concentration of this area reached the value of $6 \times 10^{19}\,cm^{-3}$, but the density of big OPs was less than in the deeper part described above. That can be explained that the most oxygen atoms segregate at extended defects forming clusters or small precipitates.

2.3 Results of electrical measurements Free electron concentration profiles of the nO_4 sample retrieved from capacitance–voltage (CV) measurements at 1 MHz are shown in Fig. 2b. A significant distinction of the profiles from the SIMS concentration profiles is obvious from the comparison of Figs. 1 and 2. The curve in Fig. 2 measured at 300 K possess two maxima in the region from 150 to 700 nm while SIMS profile is rather flat at these depths. Moreover, the shape of the free electron profile changes drastically upon cooling. This suggests that the implanted oxygen possesses different forms in different parts of the implanted region.

The concentration of the first concentration peak (from 200 to 300 nm) was as high as about $6 \times 10^{16}\,cm^{-3}$ at 300 K. It monotonically decreased down to $3.5 \times 10^{16}\,cm^{-3}$ at 100 K and did not significantly change by further lowering of the temperature. This behavior can be explained by the presence of deep levels in such region which are freeze out below 100 K and of shallow levels which can be emptied at the temperature as low as 50 K. The DLTS spectra corresponding refilling of the states in the range between 100 and 300 nm which were presented in our previous paper [10] and are not shown for brevity confirmed the validity of this assumption. The spectra consisted of the two main peaks. The emission parameters of the first one at $T = 100$ K were close to vacancy-oxygen center [14] as well as for dislocation-related center denoted as A in Ref. [15] and of the second one at $T = 200$ K denoted in Ref. [16] as DE2. We assume that both centers are vacancy-related since the depth of the free electron concentration peak at 300 nm correlates well with the position of the concentration maximum of vacancies generated by the multistep implantation as calculated by SRIM.

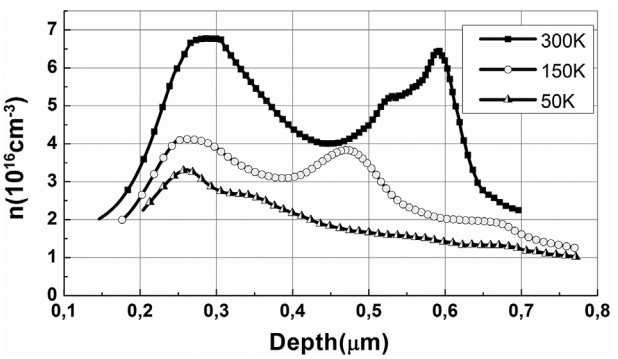

Figure 2 Temperature dependences of free electron concentration profiles of the sample nO_4 with 1000 °C pre-annealing.

In the region 300–400 nm, the concentration profile becomes weakly dependent on temperature below 200 K indicating the presence of deep levels that freeze out below this temperature and the presence of excess shallow donors with a large concentration.

Exact shape, spatial position, and the free electron concentration value of trapped electrons of the second peak area (at 600 nm at 300 K in Fig. 2) could not be defined due to the small value of capacitance at high bias reverse voltages. Nevertheless, temperature dependence in this layer differs from the near surface one since the electron concentration in this area becomes close to initial one below 100 K.

DLTS spectra corresponded to this area are shown in Fig. 3b. For the both group of the samples it consisted of the single broad maximum. For nO_4 sample with 1000 °C pre-anneal it appeared at 160 K and possessed an activation energy for electron thermoemission of $E_a = 0.3$ eV while for the sample nO_3 it was significantly broader, shifted to 210 K having $E_a = 0.35$ eV. Again there is a good correlation with temperature behavior of concentration profile since all centers in this area have to be filled with electrons below 100 K. Since the main defects found out by TEM in this region are big OPs it is naturally to ascribe observed DLTS bands to OPs electronic states.

Another difference in the electronic properties of the OPs between the samples of two groups was their sensitivity to the intense electron irradiation as it demonstrated in Fig. 3. After irradiation the concentration profiles of the sample nO_3 without pre-anneal became similar to profiles of the sample with pre-annealing shown in Fig. 2: room temperature concentration profile exhibits two peaks near the surface and at the bottom of the implanted region. Besides, the temperature-independent concentration peak which was present in nO_3 sample near OP layer (see Fig. 3a) even at 50 K disappeared at low temperatures. In contrast to that, the concentration profiles in the sample nO_4 with pre-anneal were not changed noticeably after the electron irradiation.

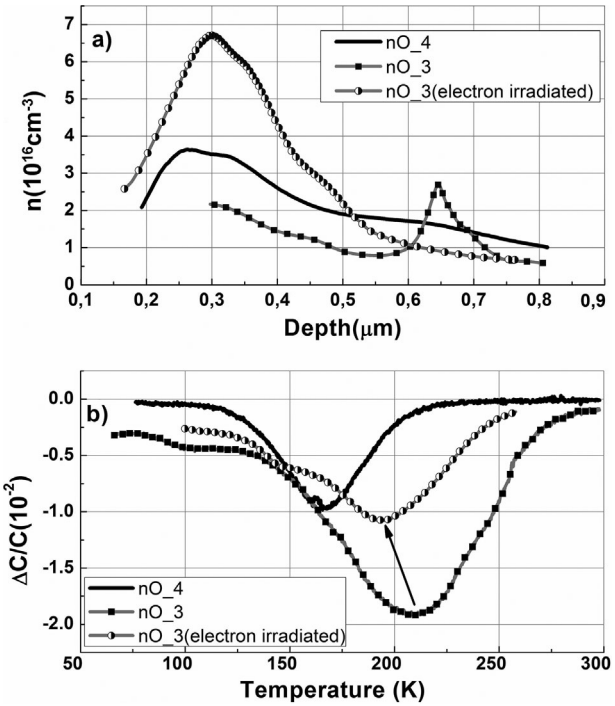

Figure 3 (a) Electron concentration profiles measured at 100 K (a) and DLTS spectra (b) of the samples nO_4 (back solid line) and nO_3 before (black squares) and after (white-black circle) electron irradiation. DLTS rate window – 200 Hz, reverse bias voltage – 5 V, pulse amplitude voltage 2 V.

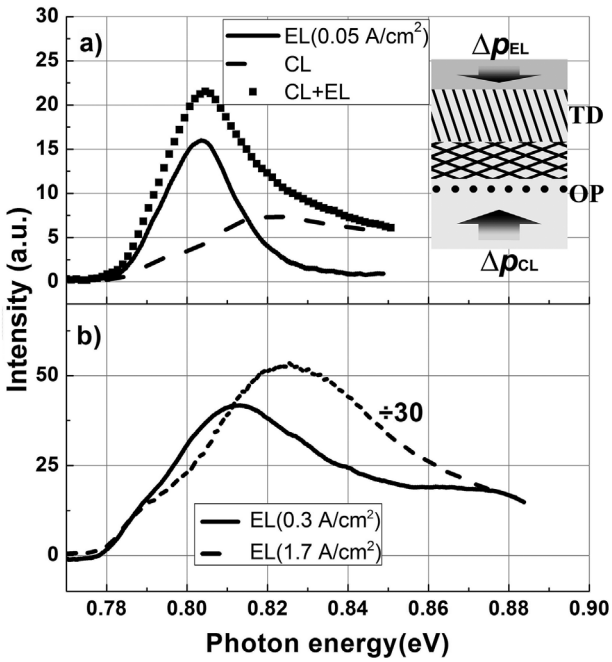

Figure 4 (a) EL (solid line) and CL (dashed line) spectra obtained on nO_4 sample. Black squares – simultaneous CL and EL excitation. Insert: arrows shows minority carrier current directions by the excitation of CL and EL. (b) EL spectra at higher injection level. The current densities are shown in the legend.

The irradiation induced changes in the concentration profiles nO_3 sample accompanied with the shift of initial temperature position of DLTS band toward lower temperature as well as with a decrease of emission energy tending to be similar to nO_4 ones (see Fig. 3b). The irradiation of the latter one resulted only in a small DLTS peak broadening of its low-temperature tail.

No marked changes in DLTS spectrum from dislocation-reach TD layer were detected upon electron irradiation.

2.4 EL and CL measurements The results presented in the previous paragraph revealed a correspondence between particular structural features and electrical properties of near surface TD and bottom OP layers of the implanted region. To define spectral contribution to the DRL from two such layers we applied two methods EL and CL based on the following consideration.

The luminescence intensity at low excitation levels is determined by the local concentration of injected minority carriers close to their source. When a forward bias is applied to the p–n junction the minority carriers are injected from p^+ injector to n-region as it is shown in the insert of Fig. 4a. At sufficiently low currents DRL should be excited predominantly near the interface of p–n junction within the region marked as TD in Figs. 1 and 4. In the area from the surface to 300 nm dislocations are dominated as it was discussed in Fig. 1.

When the sample is excited by an electron beam with an accelerating voltage of 30 kV the center of the e–h pair generation volume locates at the penetration depth of the electron beam of about 5 μm from the surface. In this case, the minority carriers reach the implantation region at the other side as shown in the insert of Fig. 4b. Therefore, in this case, the carriers primarily recombine within the deeper part of the implantation region marked as OP.

In both cases with an increase of the excitation level the luminescence from the central layer (SD + OP in Fig. 1) caused by the diverse structural defects can occur.

The luminescence measurements of the sample at 70 K are shown in Fig. 4a. The EL spectrum measured at the current density about 0.05 A cm^{-2} exhibits a narrow peak at the photon energy of 0.805 eV that corresponds well the position of D1 line of the dislocation-related luminescence [1].

CL spectrum taken at $V_{ac} = 30$ kV and the beam current of few nA is depicted as dashed line in Fig. 4a. It differs significantly from the EL spectrum consisting of the broad band with the peak energy of 0.82 eV and with the prolonged high energy tail as well as the small hillock at the energy about 0.8 eV. The spectrum obtained with the combined excitation both with injection current density of 0.05 A cm^{-2} and electron irradiation is shown in Fig. 4a with the dotted line. It coincided well with the algebraic sum of EL and CL spectra.

The results of EL measurements on the same sample measured at higher injection current densities using pulses

excitation [10] is shown in Fig. 4b. One can see that at the current density of 0.3 A cm^{-2}, the maximum position of the signal is close to D1 line dislocation-related luminescence though a long tail similar to observed with electron beam excitation is present as well. With increasing of the current EL spectrum is shifted to the higher energy and at the injection current of 1.7 A cm^{-2} its shape becomes similar to CL one. Thus, the blue spectral shift with increasing of the injection current is caused mostly by the increase of the contribution of deeper than TD layer, i.e., of SD + OP and OP layers.

It would be interesting to follow the evolution of the spectra from another side of the structure using CL technique. Unfortunately larger than used CL excitation level was not possible being limited by the SEM electron source.

It should be noted that there some minor changes in the luminescence spectra after intense prolonged electron irradiation were observed also. Their description is beyond of the scope of this paper and will be published elsewhere.

3 Summary and discussion The defect structure of the oxygen-implanted region observed with TEM on our samples differs significantly from those observed on silicon implanted with Erbium or Si and subjected by similar thermal treatment [5].

From the TEM data (Fig. 1) were found that in the near-surface region (up to 300 nm) there are only dislocations. The oxygen concentration in the area according to SIMS data was also very high ($\sim 2 \times 10^{19}$ cm^{-3}) but no visible in TEM OPs were detected. From the electron concentration profile temperature changes the density of deep dislocation-related traps can be estimated as about 3×10^{16} cm^{-3} (Fig. 2). For the dislocation density of 10^{11} cm^{-2} that gives a reasonable value of 3×10^5 oxygen/cm dislocation length. However, assumption about the homogeneous distribution of oxygen along dislocations does not explain peak-like behavior of electron concentration profile in this area. The depth of that peak coincides well with the peak of vacancy concentration calculated with SRIM. Such region in the case of the monoenergetic implant is just a half of projected range (Rp/2) which is known from the previous study of Si^+-implanted silicon to be effective getter for oxygen [17]. The reason of the enhanced gettering was ascribed to invisible for TEM, unknown vacancy-related defects. In this sense, our results are in concordance with Ref. [17] and we conclude that donor-like action is caused by oxygen vacancy complexes of thermodonor types or very small OPs which also surround dislocations.

According to the results reported for the self-implanted Si [17–19], the formation of dislocation loops and small OPs occurred mainly in the self-interstitial-rich region at Rp that is also in agreement with our results that showed a uniform layer of OPs at the depth Rp of about 700 nm (Fig. 1). Though SIMS profiles did not show a strong oxygen concentration peak in this area in our sample the electrical measurements reveal peak-like enhancement of the donor action. The absence of the SIMS peak might be due to very high concentration of electric inactive oxygen in the implantation area which is more than two orders of magnitude greater than in Cz-Si.

The presence of the first 1000 °C pre-annealing leads to an increase of the free electron concentration and of positive charge in the OPs area as well as OPs concentration near Rp. The electron irradiation also leads to changes in electrical characteristics primarily in the sample without pre-annealing. The electrical characteristics of the sample without pre-annealing after electron irradiation became similar to the electrical characteristics of the sample with pre-annealing which were rather stable under the electron beam. Similar differences in behavior of SiO_2 structure after electron irradiation the authors observed at the comparison of crystal and amorphous SiO_2 structures [20]. By luminescent measurements they showed that after electron irradiation the local crystal structure transformed into the one of a less dense amorphous structure while the luminescent measurements of the amorphous structure were not showed so strong changes. Besides, direct EDX measurement showed that under electron irradiation even at 70 K the oxygen content in SiO_x decreases so that in massive oxide silicon nanoclusters might be formed [21].

Starting from this message we propose that the difference in the properties of the two group samples is oxygen content and atomic arrangement in OPs and clusters. During implantation oxygen ions interact immediately with the radiation native point defects forming complexes and clusters. They are rather stable at 650 °C but can be destroyed at 1000 °C. After three-stages thermal treatment, such small clusters are probably transformed into nanosized platelets of few atomic layer thick with nearly perfect atomic arrangement like those that were found after long 750 °C anneal in Ref. [22] but of smaller sizes. Such platelets produce negligible, lattice strain around and are neutral. Under electron beam irradiation some of the perfect Si-O bonds become broken providing their electric activity.

During short 1000 °C pre-treatment a part of oxygen spread out from the implanted region supplying oxygen into self-interstitial reach layer where during the next annealing stages large OPs grows on the tiny dislocation loops found in Ref. [18]. Besides, the pre-anneal transforms the initial oxygen complexes into those that can survive at $T = 1000$ °C like VO_2 [23–25] which are being electrically inactive but consume a part of oxygen that resulted in its deficit in the oxygen-related extended defects finally formed by three-stage annealing.

Luminescence measurements showed significant changes depending on the method of excitation (Fig. 4). In the spectrum of EL D1 dominated. The change of the excitation type to electron irradiation resulted in a drastic broadening of the luminescence spectrum where D1 line became less pronounced and the maximum was shifted to the higher energies. A similar effect was observed in Ref. [10] when significantly higher injection current density was used for EL excitation. This implies that not the current

density itself but rather spatial inhomogeneity of the distribution of the defects of different kinds is responsible for luminescence spectrum shape.

The blue shift of the EL spectra with the increasing of the current density can be now explained by an increase of penetration depth of the holes. Due to the high density of recombination center in the implanted region the diffusion length of the injected carriers is rather small that leads to their very abrupt concentration profile. Thus, they can reach the defect and OP-rich regions when applying very high current density only. However, the recombination at the interface causing the D1 line remains present as it is seen from Fig. 4b. Thus, from the comparison of the TEM amd capacitance measurements we can conclude that the reason for blue shift of maxima EL with increasing excitation power is caused by increasing ratio of the optical transitions through the levels of the large OPs.

Acknowledgements The authors are very grateful to Vdovin V.I. for the help in TEM study. Experimental data presented in this work were obtained using the equipment of the Interdisciplinary Resource Center for Nanotechnology at St. Petersburg State University, Russia. SIMS measurements were carried out in the Center of Multi-User Equipment "Material Science and Diagnostics for Advanced Technologies" (Ioffe Institute), supported by the Ministry of Education and Science of the Russian Federation. The work was partly supported by the research grant SPbSU 11.65.40.2017.

References

[1] N. A. Drozdov, A. A. Patrin, and V. D. Tkachev, JETP Lett. **23**, 597 (1976).
[2] E. O. Sveinbjornsson and J. Weber, Appl. Phys. Lett., **69**, 2686 (1996).
[3] E. A. Steinman, A. N. Tereshchenko, V. Y. Reznik, and R. J. Falster, Phys. Status Solidi A **204**, 2238 (2007).
[4] V. Kveder and M. Kittler, Mater. Sci. Forum **590**, 29 (2008).
[5] N. A. Sobolev, Semiconductors **44**, 1 (2010).
[6] S. Pizzini, E. Leoni, S. Binetti, M. Acciarri, A. Le Donne, and B. Pichaud, Sol. St. Phen. **95–96**, 273 (2004).
[7] N. A. Sobolev, O. B. Gusev, E. I. Shek, V. I. Vdovin, T. G. Yugova, and A. M. Emel'yanov, Appl. Phys. Lett. **72**, 3326 (1998).
[8] N. A. Sobolev, A. M. Emel'yanov, V. V. Zabrodski, N. V. Zabrodskaya, V. L. Sukhanov, and E. I. Shek, Semiconductors **41**, 616 (2007).
[9] N. A. Sobolev, A. E. Kalyadin, M. V. Konovalov, P. N. Aruev, V. V. Zabrodskiy, E. I. Shek, K. F. Shtel'makh, A. N. Mikhaylov, and D. I. Tetel'baum, Semiconductors **50**, 240 (2016).
[10] D. V. Danilov, O. F. Vyvenko, N. A. Sobolev, V. I. Vdovin, A. S. Loshachenko, E. I. Shek, P. N. Aruev, and V. V. Zabrodskiy, Solid State Phenom. **242**, 368 (2015).
[11] M. A. Stevens-Kalceff, M. R. Phillips, and A. R. Moon, J. Appl. Phys. **80**, 4308 (1996).
[12] K. Bothe, R. J. Falster, and J. D. Murphy, Appl. Phys. Lett. **101**, 032107 (2012).
[13] V. I. Vdovin, N. A. Sobolev, A. M. Emel'yanov, O. B. Gusev, E. I. Shek, and T. G. Yugova, Mater. Sci. Forum **258–263**, 1521 (1997).
[14] G. D. Watkins and J. W. Corbett, Phys. Rev. **121**, 1001 (1961).
[15] P. Omling, E. R. Weber, L. Montelius, H. Alexander, and J. Michel, Phys. Rev. B **32**, 6571 (1985).
[16] V. V. Kveder, Y. A. Osipyan, W. Schroter, and G. Zoth, Phys. Status Solidi a-Appl. Res. **72**, 701 (1982).
[17] M. Tamura, T. Ando, and K. Ohyu, Nucl. Instrum. Meth. B **59**, 572 (1991).
[18] A. Agarwal, K. Christensen, D. Venables, D. M. Maher, and G. A. Rozgonyi, Appl. Phys. Lett. **69**, 3899 (1996).
[19] S. V. Koveshnikov and G. A. Rozgonyi, J. Appl. Phys. **84**, 3078 (1998).
[20] M. A. Stevens-Kalceff, Phys. Rev. Lett. **84**, 3137 (2000).
[21] R. Salh, A. von Czarnowski, and H. J. Fitting, J. Non-Cryst. Solids **353**, 546 (2007).
[22] W. Bergholz, M. J. Binns, G. R. Booker, J. C. Hutchison, S. H. Kinder, S. Messoloras, R. C. Newman, R. J. Stewart, and J. G. Wilkes, Philos. Mag. B **59**, 499 (1989).
[23] T. Hallberg and J. L. Lindstrom, J. Appl. Phys. **72**, 5130 (1992).
[24] C. Cui, X. Ma, and D. Yang, J. Appl. Phys. **104**, 123523 (2008).
[25] G. Chen, X. Ma, Y. Bai, L. Cai, and Y. Li, Electrochem. Soc. **18**, 1019 (2009).

